Proc. Indian Acad. Sci. (*Chem. Sci.*), Vol. 113, Nos 5 & 6, October–December 2001, pp 651–658

XRD and UV-Vis diffuse reflectance analysis of CeO_2–ZrO_2 solid solutions synthesized by combustion method

G RANGA RAO* and H RANJAN SAHU
Department of Chemistry, Indian Institute of Technology, Chennai 600 036, India
e-mail: grrao@iitm.ac.in

Abstract. A series of ceria-incorporated zirconia ($Ce_{1-x}Zr_xO_2$, x = 0 to 1) solid solutions were prepared by employing the solution combustion synthesis route. The products were characterized by XRD and UV-Vis-NIR diffuse reflectance spectroscopy. The materials are crystalline in nature and the lattice parameters of the solid solution series follow Vegard's law. Diffuse reflectance spectra of the solid solutions in the UV region show two intense bands at 250 and 297 nm which are assigned respectively to $Ce^{3+} \leftarrow O^{2-}$ and $Ce^{4+} \leftarrow O^{2-}$ charge transfer transitions. The two vibrational bands in 6960 cm^{-1} and 5168 cm^{-1} in the NIR region indicate the presence of surface hydroxyl groups on these materials.

Keywords. $Ce_{1-x}Zr_xO_2$ solid solutions; combustion synthesis; diffuse reflectance spectroscopy (DRS).

1. Introduction

There has been concerted research effort in the area of ceria-based materials to unravel the structural features, oxygen exchange properties, redox behaviour and enhanced catalytic activities [1–8]. CeO_2 structurally doped with Zr^{4+} ions (also La, Gd, Pr, Tb and Pb) shows better catalytic conversions for NO reduction and CO oxidation in exhaust catalysis. This is partly attributed to the participation of the redox couple Ce^{3+}–Ce^{4+} from the bulk of the zirconia-substituted ceria lattice [1–4]. When precious metals are loaded on CeO_2–ZrO_2 solid solutions, strong interactions occur between the metal particles and Ce^{4+}/Ce^{3+} ion pair in the CeO_2–ZrO_2 solid solutions resulting in substantial increase in the efficiency of redox processes at temperatures as low as 340 K [4,9]. This process involves exchangeable surface- as well as bulk-O^{2-} ions and is mainly responsible for the low-temperature redox mechanism and greater catalytic efficiency [3,4,10]. The other key factor generally considered in oxide catalysis is surface acid–base properties of oxides [11]. Attempts have been made recently to rationalize the nature of the acid–base properties of CeO_2–ZrO_2 solid solutions and their influence on catalytic reactions [5,12]. ZrO_2 is considered a versatile support material in heterogeneous catalysis due to its amphoteric character and high thermal stability [13–15]. It has been used as a single oxide or in mixed oxides as a catalyst in organic synthesis. When ZrO_2 is incorporated in the CeO_2 lattice, the resulting CeO_2–ZrO_2 solid solutions are expected to have the combined effect of both the redox and the acid–base properties of individual components. Incorporation of zirconia into ceria and vice versa modifies the surface acid–base properties involving

*For correspondence

exposed Ce^{4+} and Zr^{4+} ions (Lewis acid sites) and O^{2-} ions (Brønsted or Lewis base sites). Both CeO_2 and ZrO_2 have the same metal–oxygen stoichiometry but have different ionic characters. CeO_2 is considered to be more ionic than ZrO_2. The acid-strength of the mixed oxide may vary depending on the charge and radius of the cations as well [5]. Under mild reductive atmosphere, cerium can exist in the solid solution as Ce^{3+} and Ce^{4+} ions while zirconium exists as Zr^{4+} ions only. The acid-strength of the Ce^{4+} (radius 0·97 Å) site is expected to be higher than that of the Ce^{3+} (radius 1·14 Å) site because of the higher charge/radius ratio of the former. The zirconium ion (Zr^{4+}) radius is 0·84 Å smaller than that of the Ce^{4+} ion and it is likely to exhibit acidic nature in solid solution. Moreover, surface hydroxyl groups may also be generated due to dissociative adsorption of water on highly polar M_1–O–M_2 bonds. These hydroxyl groups may exhibit either Brønsted acidity or basicity in general. It is therefore difficult to predict quantitatively the effect of relative amounts of CeO_2 and ZrO_2 on the acid–base properties which would depend on the preparative conditions, reducing atmosphere, exposure to water and cation site distribution in the solid solutions.

Ceria-based mixed oxides, particularly CeO_2–ZrO_2 solid solutions, have been prepared both by conventional soft chemical routes [2,16] and innovative methods such as high energy ball-milling [5,17]. The activities of these materials have been tested for a variety of catalytic reactions which include NO reduction by CO [1–4], dehydration [5] and esterification reactions [12]. However, there are other methods for the preparation of substituted zirconia- and ceria-based materials with suitable physicochemical properties for liquid and vapour phase catalytic applications [5,15,18–21]. In this study, combustion synthesis has been adopted for the preparation of mixed oxide materials in short time periods of about 5 min. This method avoids the earlier cumbersome and time-consuming procedure which involves precipitation and calcination steps during the preparation of mixed oxide catalysts. The aim of the present study is to prepare and characterize ceria–zirconia solid solutions by combustion synthesis as an alternate method and to probe the surface properties of the materials produced using diffuse reflectance spectroscopy.

2. Experimental

The $Ce_{1-x}Zr_xO_2$ (x = 0·2, 0·4, 0·6, 0·8 and 1·0) solid solutions were synthesised by the combustion method following the literature procedure [15,22]. The solution containing appropriate quantities of $(NH_4)_2Ce(NO_3)_6$ and $ZrO(NO_3)_2$ salts was ignited at 350°C for combustion using carbohydrazide, CH_6N_4O, as fuel. The materials were characterised by powder X-ray diffraction using CuK_a radiation (λ = 1·5418 Å) and UV-Vis-NIR diffuse reflectance spectroscopy using Varian 5E spectrometer with $BaSO_4$ coated integration sphere. The samples were taken in the form of ~2 mm thick self supported pellets to measure the remission function $F(R_\infty)$.

3. Results and discussion

3.1 *XRD analysis*

The X-ray diffraction pattern for combustion synthesized $Ce_{1-x}Zr_xO_2$ solid samples are given in figure 1. The XRD pattern shows three main reflections (111), (200) and (220) characteristic of CeO_2 cubic phase with fluorite structure (ref. JCPDS card 34–394). In the case of ZrO_2, both monoclinic (M) and tetragonal (T) ZrO_2 phases are evidenced in

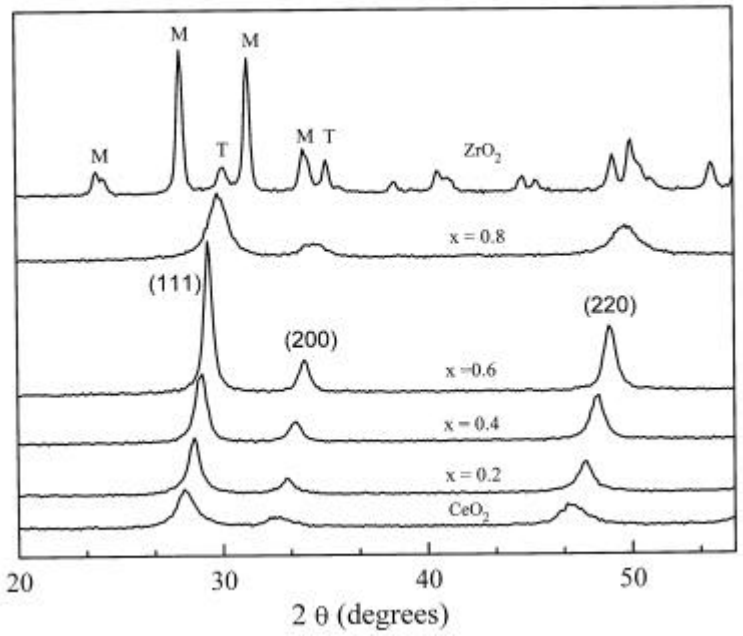

Figure 1. X-ray diffraction patterns of CeO_2, $Ce_{1-x}Zr_xO_2$ (x = 0·2, 0·4, 0·6, 0·8) and ZrO_2 powders prepared by combustion method.

the combustion product and the relative amounts of these two phases depend on the amount of fuel used in the combustion mixture[15]. On the other hand, X-ray analysis of mixed oxide products shows the formation of homogeneous $Ce_{1-x}Zr_xO_2$ solid solutions. The XRD lines of the solid solutions are similar to those of CeO_2 indicating the stabilisation of the fluorite structure by zirconia substitution. All the three X-ray reflections have been shifted gradually to higher values of 2θ with increase in zirconium content in the solid solution. The $Ce_{1-x}Zr_xO_2$ solid solutions prepared by other methods, such as high energy ball milling and co-precipitation, also show the same behaviour which is ascribed to the insertion of zirconium ions of smaller radius into the cubic lattice of CeO_2 resulting in the contraction of its cell parameter[17,22,23]. Accordingly, the lattice parameter is found to decrease linearly from 0·544 nm to 0·520 nm with increase in ZrO_2 content following the Vegard law. In addition, the widths of XRD lines of CeO_2 and $Ce_{1-x}Zr_xO_2$ solid solutions are broader, except for $x = 0{\cdot}6$ sample, compared to ZrO_2 lines. The particle sizes calculated using Scherrer formula of the solid solutions are in the range 10–20 nm.

3.2 *UV-Vis-NIR diffuse reflectance spectroscopy*

We have investigated the surface structure of the $Ce_{1-x}Zr_xO_2$ powders by UV-Vis-NIR diffuse reflectance spectroscopy. Diffuse reflectance spectroscopy and its application to study metal oxides have been reviewed recently[24]. Briefly, this technique is based on the reflection of light in the ultraviolet (10–420 nm), visible (420–700 nm) and near-infrared (700–2500 nm) regions by a powder sample. In a diffuse reflectance spectrum (DRS), the ratio of the lights scattered from a (> 2–3 mm) thick layer of sample and an ideal non-

absorbing reference sample is measured as a function of the wavelength λ (i.e. $F_{SKM}(R_\infty)$ vs λ in nm). The relation between the diffuse reflectance of the sample (R_∞), absorption (K) and scattering (S) coefficients are related by the Schuster–Kubelka–Munk (SKM) remission function:

$$F_{SKM}(R_\infty) = (1 - R_\infty)^2/2R_\infty = K/S.$$

The SKM remission function relates the experimentally determined diffuse reflectance of a thick sample to K and S. At constant S, $F_{SKM}(R_\infty) \propto K$ and a plot of $F_{SKM}(R_\infty)$ vs concentration of absorbing species should be a straight line passing through the origin. This linear relationship can be used for quantitative studies on powder samples of infinite layer thickness containing uniformly distributed metal ions in low concentration. The remission function also depends strongly on particle size for weak absorbers but not for strong absorbers which absorb almost all the incident photons. DRS has been used extensively to study ceria-based materials and transition metal oxides (e.g. dispersed chromium oxide)[24–30] to obtain information on surface coordination and different oxidation states of metal ions by measuring *d–d*, *f–d* transitions and oxygen–metal ion charge transfer bands. However, this technique has limitations due to the difficulty in interpreting the large bandwidths and specular reflectance often observed in the spectra.

3.2a *UV region:* Crystalline cerium dioxide has a band gap of 3·1 eV and absorbs strongly in the UV region with the absorption threshold near $\lambda = 1240/E_g = 400$ nm (25 000 cm^{-1}). On the other hand, *m*-ZrO_2 has two direct interband transitions at 5·93 eV and 5·17 eV, which is quite different from the behaviour of ceria and absorbs light at $\lambda \leq 240$ nm with an absorption threshold edge near 240 nm (41666 cm^{-1})[15,31]. The other phase is *t*-ZrO_2 which has a band gap of 5·1 eV and the absorption threshold edge position is expected at 240 nm[32]. It is therefore possible to identify zirconia phases in the UV range of DRS. Doping of transition metal ions such as Fe^{3+} into zirconia increases the wavelength of absorption into the visible region (lower energy) and the onset of absorption is red-shifted due to the introduction of energy levels in the interband gap[33]. The band gap of a material can be estimated from the absorption edge wavelength of the interband transition. According to Bensalem *et al*[26], the UV absorption edge wavelength is very sensitive to the particle size of semiconductor materials such as ceria and zirconia. When crystallite size is below 10 nm, the band gap energy increases with decreasing the crystallite size and the absorption edge of the interband transition is blue-shifted. Such blue shifts of the interband transition energy (i.e. band gap) are clearly seen in the UV region of DRS for very small ceria particles of 1–5 nm size[25,27]. In addition to a blue shift, DRS shows four narrow bands in the range of 250–350 nm for small CeO_2 crystallites (<2 nm) and can detect <100 ppm of cerium in a supported powder catalyst. These bands are attributed to localized O–Ce charge transfer transitions involving a number of surface Ce^{4+} ions with different coordination numbers[27]. The coordination number of surface Ce^{4+} ion can vary between four and eight, the latter being the coordination number of bulk Ce^{4+}. Some of the important UV-Vis bands and their assignments for ceria and zirconia materials from our work and literature are presented in table 1. The $Ce^{3+} \rightarrow Ce^{4+}$ charge transfer transition (17 000 cm^{-1}) has been specifically used to follow the degree of reduction which is an important factor related to the oxygen-storage capacity of ceria[3,30]. The 4*f*–5*d* transitions occur prominently in the UV region (~200–250 nm) for isolated Ce^{3+} ions on the surface or in other oxide matrices.

Table 1. UV-Vis diffuse reflectance charge transfer band maxima (in nm) for ceria and zirconia materials.

Nature of species and transition*	Reference number(s)						This work
	25	26	27	28	30	31, 33	
LC surface Ce^{3+}–O^{2-}, $Ce^{3+} \leftarrow O^{2-}$	–	265	250–350	255	–	–	250
LC surface Ce^{4+}–O^{2-}, $Ce^{4+} \leftarrow O^{2-}$	275	280	250–350	278	–	–	297
Surface Ce^{3+}/Ce^{4+} pair, $Ce^{3+} \rightarrow Ce^{4+}$	650	588	–	–	588	–	–
$f \rightarrow d$ transitions of Ce^{3+} species	–	–	–	–	200–300	–	208–218
Interband transitions in CeO_2	340	325, 350	320–350	313	–	–	320–340
LC surface *t*-ZrO_2, $Zr^{4+} \leftarrow O^{2-}$	–	–	–	–	–	320–325	~325
Interband transitions in *m*-ZrO_2	–	–	–	–	–	209, 240	218, 228

*LC = low coordination

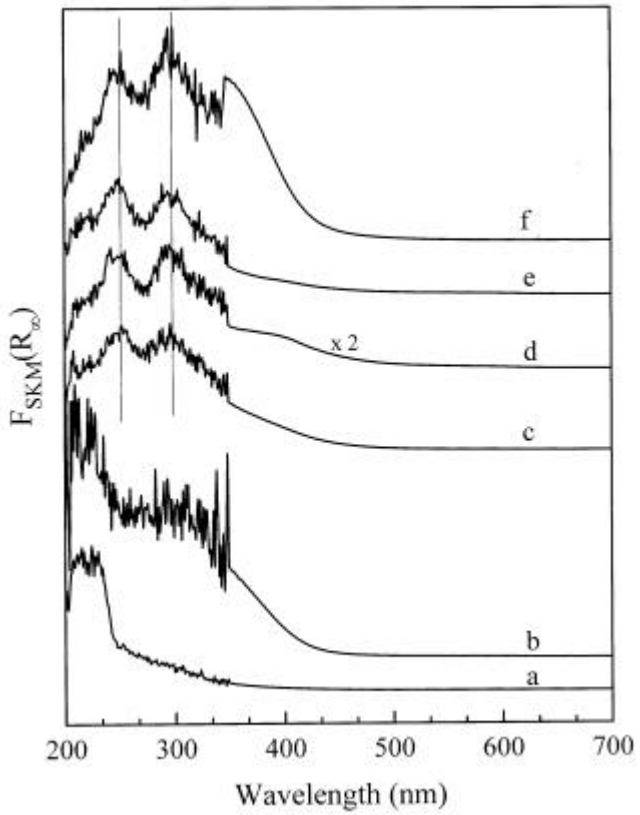

Figure 2. UV-diffuse reflectance spectra of (a) ZrO_2, (b) 1:1 mechanical mixture of CeO_2 and ZrO_2, (c–e) $Ce_{1-x}Zr_xO_2$ (x = 0·8, 0·6 and 0·4) and (f) CeO_2.

The DRS spectra of CeO_2, ZrO_2 and various $Ce_{1-x}Zr_xO_2$ solid solutions prepared by combustion method are given in figure 2. Several absorption bands are observed in the UV region between 200 and 420 nm. The DRS of ZrO_2 sample shows two absorption peaks at 228 and 214 nm with an absorption edge at 245 nm (5·06 eV) as expected for a predominantly *m*-ZrO_2 sample seen in XRD (figure 1). It is to be noted that the UV absorption features are sensitive to the presence of mixed phases of zirconia, defects, impurities and the amorphous nature of the sample[33]. The 1:1 mechanical mixture of CeO_2 and ZrO_2 exhibits spectral features composed of two separate absorption thresholds characteristic of CeO_2 (400 nm) and ZrO_2 (240 nm) components. However, the DRS spectra shown in figure 2 for $Ce_{1-x}Zr_xO_2$ solid solutions ($x = 0·0$, $0·4$, $0·6$ and $0·8$) are strikingly different and resolve four bands at 208, 250, 297 and ~335 nm. For solid solutions, the intensities of the two strong bands at 250 and 297 nm seen in the CeO_2 spectrum are reduced without any change in the band positions. The UV-Vis spectral features of CeO_2 with the fluorite lattice and Zr^{4+}-substituted solid solutions with modified fluorite lattice are similar and may be assigned to $Ce^{3+} \leftarrow O^{2-}$ (250 nm) and $Ce^{4+} \leftarrow O^{2-}$ (297 nm) charge transfer transitions[26–28]. It has been reported[34] that the introduction of isovalent cation-like Zr and Hf into the *fcc* cell of ceria results in nonstoichiometric fluorite structure. Recent TPR data provides evidence for such modified CeO_2 particles containing variety of low coordinated surface and bulk cations associated with lattice defects[4,34]. Therefore the DRS bands discussed above are likely to occur due to localized O–Ce charge transfers from the nonstoichiometric fluorite

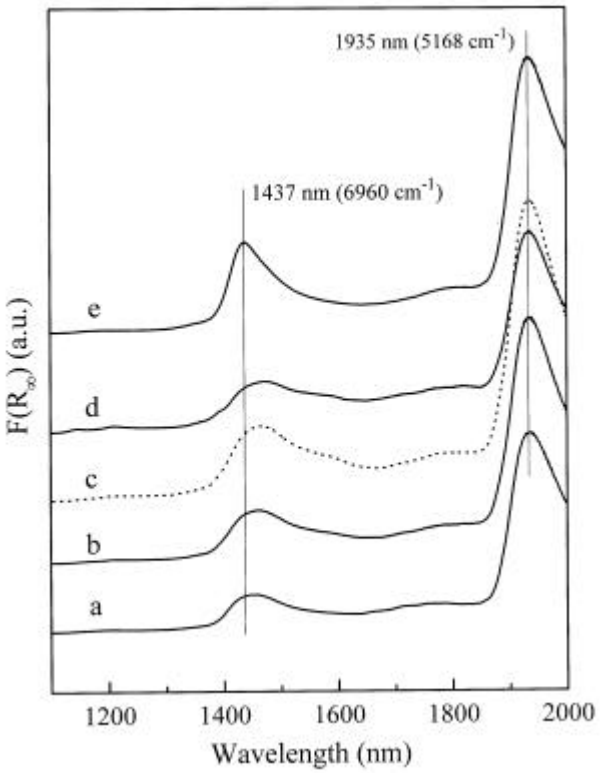

Figure 3. NIR-diffuse reflectance spectra of (a) ZrO_2, (b–d) $Ce_{1-x}Zr_xO_2$ ($x = 0·8, 0·6$ and $0·4$) and (e) CeO_2.

Table 2. Approximate overtone and combination band positions (in nm) for H_2O and OH groups in the region 1100–2000 nm [37].

Assignment	H_2O	OH
$2n_1$	1400	1400
n_1 + M–O–H bend	–	1900–2100
$n_2 + n_3$	1800–1900	–

structures. The weak band between 208 and 218 nm seems to be related to 4*f*–5*d* transition from Ce^{3+} ions embedded in the zirconia matrix [35]. The broad shoulder-type band at 320–340 nm on the higher wavelength side in the DR spectra may consist of interband and $Zr^{4+} \leftarrow O^{2-}$ transitions of the substituted fluorite lattice (table 1). When CeO_2 is mechanically mixed with ZrO_2 the two intense DRS features disappear and are replaced with a very broad band. Bensalem *et al* [25,27] reported similar results for a mechanically mixed sample containing diluted CeO_2 (2%) in SiO_2.

3.2b *NIR region:* The NIR portion of the DRS covers the overtones and combination bands of the fundamental stretching frequencies of surface molecular groups such as H_2O and O–H [36–38]. These bands are smaller in intensity and excellently measured in diffuse reflectance rather than in transmission mode because of the large scattering involved in the NIR region. The NIR–DRS spectra for combustion synthesized samples are presented in figure 3. The $F(R_\infty)$ (i.e. absorption) function in the region 1100–2500 nm essentially shows the presence of water and hydroxyl groups in solid materials [37]. Some of the reported spectral properties of H_2O and OH in the NIR region are collected in table 2. Based on these data, the two vibrational bands at 1437 and 1935 nm in the DR–NIR spectra of $Ce_{1-x}Zr_xO_2$ samples are attributed to the combination and overtone bands mainly from the surface hydroxyl groups and to a smaller extent from water. Surface hydroxyl groups are known to occur on zirconia and ceria [30] with IR bands at 3652 and 3633 cm^{-1} and 3772 and 3668 cm^{-1} respectively, and they produce the overtone and combination bands in the NIR region. Further, the intensity of the peaks in this region depends strongly on water and surface hydroxyl content [37]. Among the solid solutions investigated, the $Ce_{0.4}Zr_{0.6}O_2$ sample shows higher hydroxyl content. The peak at 1437 cm^{-1} is broad and resembles that of ZrO_2. This is an indication that the OH groups are primarily associated with Zr^{4+} ions in the solid solutions and may behave as Brønsted acid or base sites in catalytic reactions.

4. Conclusions

Combustion synthesis has been used as an alternate method to prepare $Ce_{1-x}Zr_xO_2$ powders and the formation of solid solutions is confirmed by XRD. UV-Vis-NIR diffuse reflectance measurements show the $Ce^{3+} \leftarrow O^{2-}$ and $Ce^{4+} \leftarrow O^{2-}$ charge transfer transitions in the UV region and combination and overtone bands of surface hydroxyl species in the NIR region. The DRS spectral features of the solid solutions indicate the presence of surface Ce^{3+}–O^{2-} and Ce^{4+}–O^{2-} species and OH groups attached primarily to Zr^{4+} ions.

Acknowledgments

Financial support from the Council of Scientific and Industrial Research, New Delhi is gratefully acknowledged. We thank the Regional Sophisticated Instrumentation Centre, Indian Institute of Technology Madras for providing the experimental facilities.

References

1. Trovarelli A 1996 *Catal. Rev. Sci. Eng.* **38** 439
2. Ranga Rao G, Fornasiero P, Kašpar J, Meriani S, Di Monte R and Graziani M 1995 *Stud. Surf. Sci. Catal.* **96** 631
3. Fornasiero P, Ranga Rao G, Kašpar J, Erario F L and Graziani M 1998 *J. Catal.* **175** 269
4. Ranga Rao G 1999 *Bull. Mater. Sci.* **22** 89
5. Cutrufello M G, Ferino I, Solinas V, Primavera A, Trovarelli A, Auroux A and Picciau C 1999 *Phys. Chem. Chem. Phys.* **1** 3369
6. Overbury S H, Mullins D R and Glavee G N 1998 *Catal. Lett.* **51** 133
7. Narula C K, Haack L P, Chun W, Jen H W and Graham G W 1999 *J. Phys. Chem.* **B103** 3634
8. Baker R T, Bernal S, Blanco G, Cordon A M, Pintado J M, Pintado J M, Rodriguez-Izquierdo J M, Fally F and Perrichon V 1999 *Chem. Commun.* 149
9. Fornasiero P, Kašpar J and Graziani M 1997 *J. Catal.* **167** 576
10. Bera P, Patil K C, Jayaram V, Subbanna G N and Hegde M S 2000 *J. Catal.* **196** 293
11. Busca G 1999 *Phys. Chem. Chem. Phys.* **1** 723
12. Sugunan S and Varghese B 1998 *Indian J. Chem.* **A37** 806
13. Yamaguchi T 1994 *Catal. Today* **20** 199
14. Aramendia M A, Borau V, Jimenez C, Marinas J M, Porras A and Urbano F J 1999 *J. Catal.* **183** 240
15. Ranjan Sahu H and Ranga Rao G 2000 *Bull. Mater. Sci.* **23** 349
16. Brayner R, Ciuparu D, da Cruz G, Mfievet-Vincent F and Bozon-Verduraz F 2000 *Catal. Today* **57** 261
17. Trovarelli A, Zamar F, Llorca J, Leitenburg C, Dolcetti G and Kiss J T 1997 *J. Catal.* **169** 490
18. Upadhya T T, Katdare S P, Sabde D P, Ramaswamy V and Sudalai A 1997 *J. Chem. Soc., Chem. Commun.* 1119
19. Ramana D V and Pillai C N 1969 *Can. J. Chem.* **47** 3705
20. Johnstone R A W and Wilby A H 1985 *Chem. Rev.* **85** 129
21. Shibagaki M, Takahashi K and Matsushita H 1988 *Bull. Chem. Soc. Jpn.* **61** 3283
22. Aruna S T and Patil K C 1998 *Nano-Structured Mater.* **10** 955
23. Sergent N, Lamonier J and Aboukais A 2000 *Chem. Mater.* **12** 3830
24. Weckhuysen B M and Sehoonheydt R A 1999 *Catal. Today* **49** 441
25. Rakai A, Bensalem A, Muller J C, Tessier D and Bozon-Verduraz F 1992 *New frontiers in catalysis, Proc. 10th Int. Cong. Catal.* (ed.) L Guczi (Amsterdam: Elsevier) p. 1875
26. Bensalem A, Muller J C and Bozon-Verduraz F 1992 *J. Chem. Soc., Faraday Trans.* **88** 153
27. Bensalem A, Bozon-Verduraz F, Delamar M and Bugli G 1995 *Appl. Catal.* **A121** 81
28. Zaki M I, Hussein G A M, Mansour S A A, Ismail H M and Mekhemer G A H 1997 *Colloids Surfaces* **A127** 47
29. Brayner R, Ciuparu D, da Cruz G M, Fievet-Vincent F and Bonzon-Verduraz F 2000 *Catal. Today* **57** 261
30. Binet C, Bardi A and Lavalley J C 1994 *J. Phys. Chem.* **98** 6392
31. Aita C R and Kwok C 1990 *J. Am. Ceram. Soc.* **73** 3209
32. Scheithauer M, Grasselli R K and Knözinger H 1998 *Langmuir* **14** 3019
33. Navío J A, Hidalgo, Colón G, Botta S G and Litter M I 2001 *Langmuir* **17** 202
34. Ozawa M 1998 *J. Alloys Comp.* **275** 886
35. Barrie J D, Momoda L A, Dunn B, Gourier D, Aka G and Vivien D 1990 *J. Solid State Chem.* **86** 94
36. Lindberg J F and Snyder D G 1972 *Am. Minerol.* **57** 485
37. Coyne L M, Bishop J L, Scattergood, Banin A, Carle G and Orenberg J 1990 *Spectroscopic characterization of minerals and their surfaces: ACS Symposium Series 415* (eds) L M Coyne, S W S McKeever and D F Blake (Washington: ACS) p. 407
38. Delgass W N, Haller G L, Kellerman R and Lunsford J H 1979 *Spectroscopy in heterogeneous catalysis* (New York: Academic Press) p. 126